Heat Generation Patterns and Temperature Profiles in Electroslag Welding

T. DEBROY, J. SZEKELY, AND T. W. EAGAR

A formulation is presented to calculate, in three dimensions, the important process parameters such as the voltage profiles, heat generation patterns and temperature profiles in the slag and metal phases for an electroslag welding system. It is shown that the current is significantly larger for the electroslag welding process than that of the electroslag refining process operating with equivalent slag, electrode and other geometrical variables. Calculations show that the heat generation patterns are highly sensitive to the geometrical location of the electrode in the slag and that a relatively minor error in the alignment of the electrode can cause a major asymmetry in the heat generation pattern. The temperature fields in the slag and the metal phases are calculated in three dimensions and the roles played by various factors on the heat balance are assessed. The computation accounts for the transport of heat from the slag to the metal phase by the liquid metal drops, the energy loss due to electrolysis and the energy required for the heating of the cold slag charge. Using the computed values of the weld rate the possible decrease in the heat input due to a) the decrease of the plate gap and b) the use of multiple electrodes is calculated. The values of heat input obtained from independent experiments are compared with model predictions. Possible effects of imposing an external magnetic field during the welding are examined.

I. INTRODUCTION

THE electroslag welding process is a potentially attractive operation for the welding of thick plates, needed in the construction of ships, storage tanks, pressure vessels, bridges, buildings and other structures.

Most of the earlier work has been carried out in the U.S.S.R., which is well documented;[1] in addition useful work has been done also by the British Welding Institute[2] and by the U.S. Steel Corporation.[3]

However, in all this previous work emphasis has been placed on the physical characterization of the weld, for a variety of operating conditions and rather less attention has been paid to the representation of the more fundamental aspects of the heat and fluid flow phenomena that are associated with electroslag welding. There appears to be agreement in the welding literature that the size of the heat affected zone, the sequence of solidification and the slag metal reactions play a key role in determining the weld properties. It is also appreciated that the size, shape and nature of the weld pool is a key factor in the production of sound welds. The work to be described in the present paper is part of a program of research which is addressed to the development of an improved fundamental, quantitative understanding of the physical factors that govern the electroslag welding process.

From a physical standpoint the electroslag welding process involves heat transfer accompanying phase change, which is markedly influenced by the fluid flow phenomena in the weld pool, driven by both thermal natural convetion and by an electromagnetic force field in a system which is truly three dimensional. The development of a fully comprehensive representation of this system would be a very difficult task so that the approach adopted is to highlight certain key aspects of the problem. In a previous paper, we examined the role of the electromagnetic and the buoyancy fields in determining the velocity and the temperature profiles in the weld pools, for idealized, mathematically two-dimensional (axisymmetrical or plate-like) systems.[4]

It was found that the buoyancy and the electromagnetic forces produce vigorous agitation in the molten weld pool and that the nature of this agitation is quite markedly affected by the geometry. When the current field is nonparallel, as is the case with wire electrodes, the electromagnetic force field plays a major role, while for parallel fields, as produced by flat plates, the flow field is driven essentially by buoyancy forces.

While this previous work established the existence of vigorous agitation in the weld pool and indicated the important role played by the system geometry, the need for the mathematically two-dimensional representation (mandated by the complexity of the electromagnetic force field and in particular the fluid flow field equations) precluded the detailed study of the geometric factors.

The purpose of the present paper is to pursue the same problem from a slightly different angle, by examining the heat generation patterns and the resultant temperature distribution in truly three-dimensional systems. A major motivation for extending the study to three dimensions is provided by the fact that this approach enables one to examine various important facets of the problem, such as the effect of closely spaced multiple electrodes, misalignment of the electrodes and the use of narrow gaps on the heat generation pattern and on the net heat input required. These problems are thought to be of great practical interest. The tradeoff inherent in the examination of this rather

T. DEBROY, formerly with the Department of Materials Science and Engineering, Massachusetts Institute of Technology, is now Assistant Professor of Metallurgy, Penn. State University, University Park, PA 16802. T. W. EAGAR and J. SZEKELY are Associate Professor and Professor, respectively, Department of Materials Science and Engineering, Massachusetts Institute of Technology, Cambridge, MA 02139.

Manuscript submitted October 15, 1979.

ISSN 0360-2141/80/1211-0593$00.75/0

more complex problem has been the assumption of neglecting convective effects, or rather, allowing for the effect of convection through the use of an effective thermal conductivity. It is thought that by combining these two approaches useful insight may be obtained into the complex multifaceted problem, while obviating the need for very major expenditures for computer time.

FORMULATION

A schematic diagram of the ESW process is shown in Fig. 1. A consumable wire electrode is fed continuously into a molten slag pool, which is resistively heated by current passing from the electrode, through the molten slag pool, the metal pool to the base plates. The electrical conductivity of the slags is significantly smaller than that of the metals and as a result, practically all of the heat is generated within the slag phase. During welding, the wire electrode melts in the slag phase and the molten metal drops descend to the metal pool, displacing the slag pool vertically upwards; solidification of the molten pool takes place joining the metal plates. Two water cooled copper shoes provide surfaces through which a portion of the heat is extracted. Fluid motion in the slag and metal phases are generated due to the electromagnetic forces resulting from the current and the buoyancy forces due to the local temperature differences. The transport of thermal energy takes place by conduction and convection. Molten metal drops falling through the slag layer carry a portion of the heat from the slag to the metal phase. Furthermore, the addition of cold slag may also adsorb heat from the slag phase. It follows that the proper modeling of the system requires statement of the equations describing these features in three dimensions in order that the temperature field in the system can be adequately described. In the previous paper a two-dimensional representation was developed, where account was taken of the electromagnetic force field, of buoyancy forces, of fluid flow phenomena and of convective heat transfer.

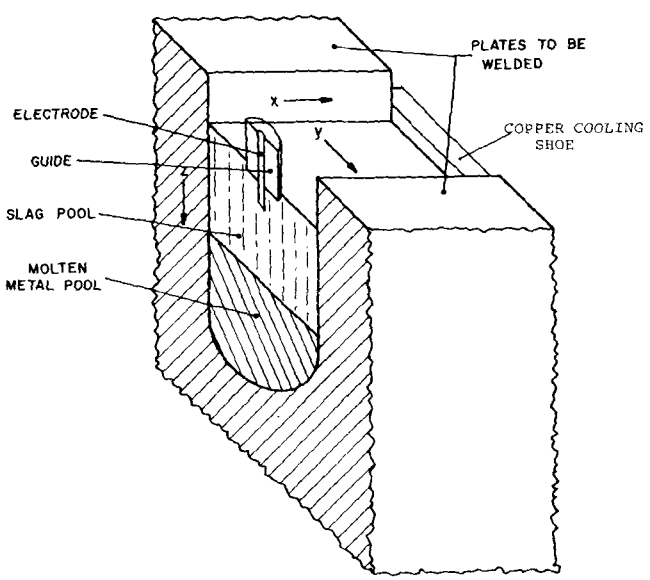

Fig. 1—Geometrical situation in the ESW process.

In the present work allowance will be made for the three-dimensional nature of the problem, but the attention will be restricted to the calculation of the electric field, of the heat generation pattern and of the conductive heat flow. However, an approximate allowance will be made for the effect of convection, through the use of an effective thermal conductivity.

THE HEAT GENERATION PATTERN

In the calculation of the heat generation pattern we shall assume that all the voltage drop occurs across the slag layer, which is reasonable, because the electric resistance of the slag phase is of the order of a few thousand times that of the metal.

The local heat generation pattern may be obtained through the solution of the following set of equations:

$$\mathbf{J} = \sigma \mathbf{E} \text{ (Ohm's Law)} \quad [1]$$

where $\mathbf{J}$ is the current density in A/m^2, σ is the electrical conductivity of the slag in (Ohm m)$^{-1}$, $\mathbf{E}$ is the electric field in V/m.

The electric field $\mathbf{E}$ may be expressed in terms of a scalar potential ϕ

$$\mathbf{E} = -\nabla \phi \quad [2]$$

The conservation of current is expressed as

$$\nabla (\sigma \nabla \phi) = 0 \quad [3]$$

The value of local heat generation rate Q_g is readily expressed as:

$$Q_g = (\mathbf{J} \cdot \mathbf{E}) \times 0.239 \times 10^{-3} \quad [4]$$

where Q_g is expressed in Kcal/m^{3}s.

The boundary conditions of Eqs. [1] to [3] are given in Appendix A.

TEMPERATURE PROFILES IN THE SLAG AND METAL PHASES

In the present work the temperature profiles in the slag and metal phases are calculated by solving a modified form of the heat conduction equation in three dimensions. The effect of convection is accounted indirectly by the use of enhanced or effective values of thermal conductivity for the slag and metal phases. The conduction equation is solved in the following form:

$$\nabla (k_{eff} \nabla T) + Q_s = 0 \quad [5]$$

This type of equation has to be written for both the slag and for the metal phase.

The values of k_{eff}, the effective conductivity, depend on the intensity of liquid circulation and the molecular conductivity values in the slag and the metal phases. Q_s, the heat source (or sink) term, embodies i) the resistive heating in the slag phase, ii) the appropriate contribution of the liquid metal drops to the process of convective heat transfer from the slag to the metal phase, iii) the energy requirement for the heating of the cold flux additions, and iv) the energy necessary for the electrolysis of the slag.

The magnitude of Q_s for the slag and the metal phases is given by:

$$Q_s = Q_g(1 - Q_d/Q_t - Q_{slr}/Q_t - Q_{elch}/Q_t)$$
for the slag phase
$$= Q_d/V_m \text{ for the metal phase} \quad [6]$$

In the above equation Q_d is the heat transfer rate from the molten slag to metal by the liquid metal drops expressed in kcal/s. The calculation procedure for Q_d is described in Appendix B. Q_t is the total heat generation rate in the slag phase in kcal/s in the absence of any electrolysis in the slag and is readily calculated by integrating the spatial distribution of the local values of heat generation rate, Q_g, over the region occupied by the liquid slag. Q_{slr} is the rate of heat requirement for preheating and melting of the cold slag and is calculated using Eq. [7]. Q_{elch} is the heat equivalent of the energy consumption rate for the electrolysis of the molten slag in kcal/s. It will be discussed later that an accurate assessment of this term is not straightforward. In the present work, a rough estimate of this term has been made by application of Faraday's Law. V_m represents the volume of the liquid metal pool. Q_{slr}, the rate of heat requirement to preheat and melt the cold slag charged during welding is given by the following equation:

$$Q_{slr} = W_{slr}[C_{psl}(T_{slav} - T_a) + \Delta H_{sl}] \quad [7]$$

where W_{slr} is the rate of slag charging in kg/s, C_{psl} is the average specific heat of the slag in kcal/kg K, T_{slav} and T_a are average temperatures of the slag and the ambient temperature respectively, ΔH_{sl} is the latent heat of fusion of slag in Kcal/kg.

The rate of slag charging W_{slr} is calculated by using Eq. [8]:

$$W_{slr} = W_{sl}/t_{fin} \quad [8]$$

where W_{sl} is the total weight of the slag charged, t_{fin} is the total time required to finish the weld and is calculated from the following relationship:

$$t_{fin} = V_{cavity} \cdot \rho_m B_f/m \quad [9]$$

where V_{cavity} is the initial volume of the weld cavity, ρ_m is the density of the weld metal, B_f is the "bulging factor," a dimensionless parameter to account for the difference between the actual weld volume and the initial weld cavity volume. Its value is taken as 1, unless evaluated from the experimental data. m is the electrode melting rate in kg/s. The calculation scheme for the electrode melting rate is discussed next.

ELECTRODE MELTING

In the present work the melting rate of the electrode is calcuated by using a heat balance of the following form:

$$Q_{el} = Q_t - Q_d - Q_{slr} - Q_{slpl} - Q_{slcu} - Q_{slm} - Q_r - Q_{elch} \quad [10]$$

where Q_{el} is the heat transfer rate from the slag to the electrode expressed in kcal/s, Q_{slpl}, Q_{slcu}, and Q_{slm} are the rate of heat transfer from the liquid slag to the base plate, copper shoe and the liquid metal pool respectively. These quantities are calculated from the temperature field by integrating the local values of surface heat flux over the appropriate surface. Q_r is the radiation loss from the top surface of the liquid slag in kcal/s, and is calculated by integrating the local values of heat flux at this surface.

Of the quantities appearing in the right hand side of Eq. [10], Q_t is evaluated after the calculation of voltage distribution in the slag phase. Other quantities appearing on the right hand side of Eq. [10] are evaluated iteratively along with the evaluation of temperature field. The melting rate of the electrode is calculated from the following relationship:

$$Q_{el} = m[C_{pm}(T_{lm} - T_a) + \Delta H_m] \quad [11]$$

COMPUTATIONAL METHOD AND RESULTS

In the following we shall present a brief account of the computational procedure and a selection of the computed results, describing the heat generating patterns, the temperature profiles and the heat input rates for a variety of operating conditions.

Computational Procedure

Because of the formulation adopted, the electric field equations and the heat flow equations are uncoupled. For this reason the field equations, *viz* Eqs. [1] to [3] are solved first, using a finite difference form. A central difference scheme involving nonuniformly spaced fixed rectangular grids is used. Irregular boundaries are approximated by judicious choice of grids. For example, the circular cross section of the electrode is represented by a regular octagon. An iterative scheme involving line by line solution procedure is employed. A particular version of Gaussian elimination technique known as tridiagonal matrix alogrithm is used. The total number of grid points used ranged from 2160 to 4004 depending on the nature of the system. (A smaller number of grid points was found adequate for symmetrical systems).

Having obtained Q_g, the spatially distributed heat generation pattern, attention could be focused on the solution of Eq. [5]. This equation had to be solved in an iterative manner, using a scheme similar to the one used for the solution of field equations. MIT's IBM 370 Digital Computer was used, and the total computer time requirement per run was of the order of 80 s.

Computed Results

The property values used in the computation are summarized in Tables I and II. More specifically, Figs. 1 to 7 have been calculated using the values given in Table I, while Table II contains the values which have been used for the computation of Figs. 8 to 11.

It is noted that the thermal conductivity of liquid slags depends on the temperature. However, we found

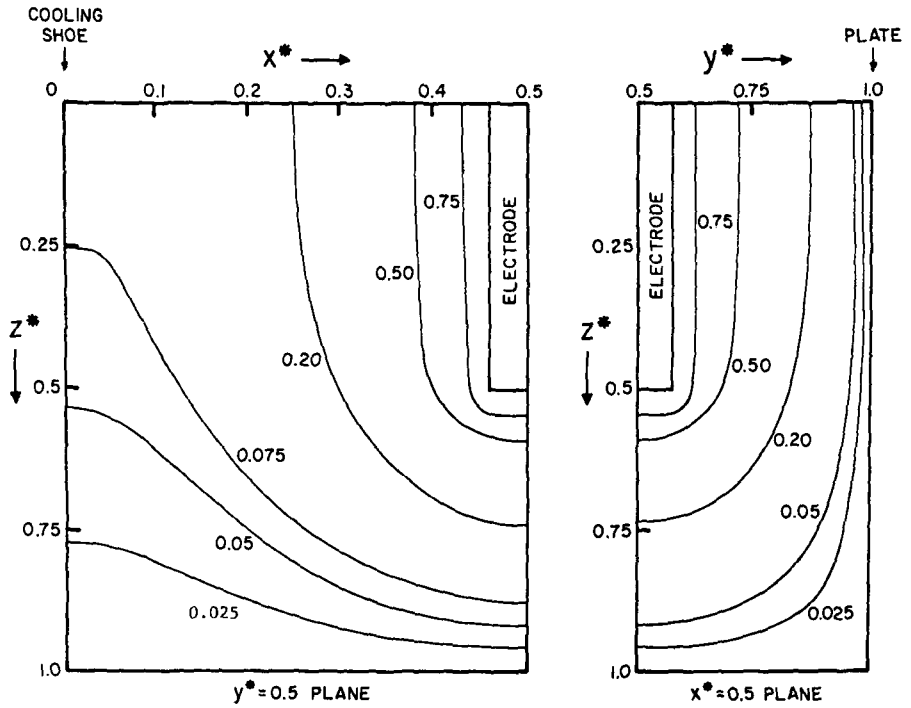

Fig. 2—Values of $(\phi - \phi_m)/(\phi_{el} - \phi_m)$ at two middle planes for the ESW process.

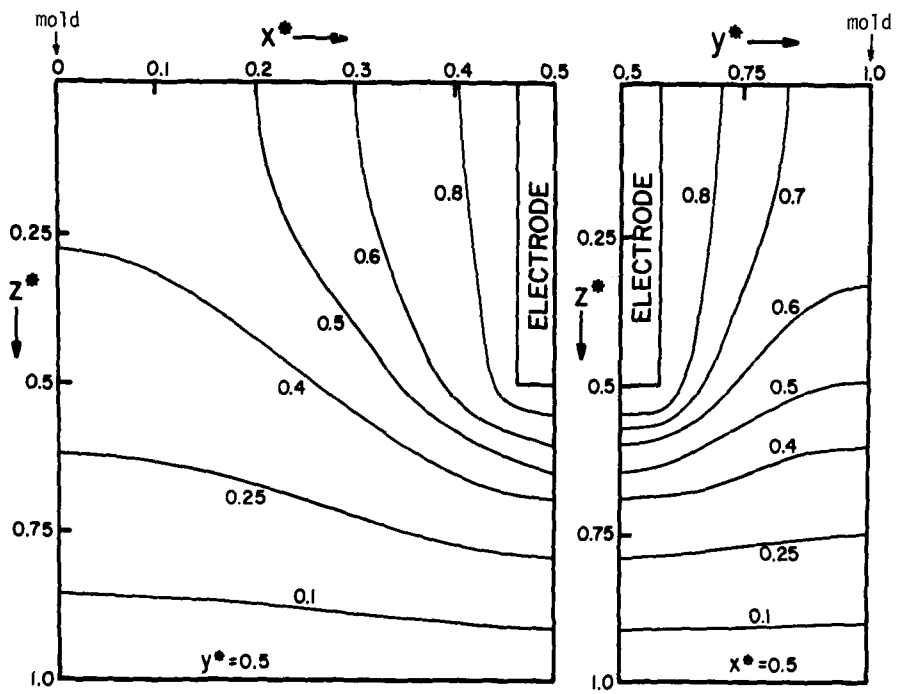

Fig. 3—Values of $(\phi - \phi_m)/(\phi_{el} - \phi_m)$ at two middle planes for the ESR process.

that the most important factor in determining the voltage profiles is the system geometry. The effect of temperature dependence of electrical conductivity of the slag on the isopotentials was examined[9] for a relatively simpler, two dimensional case in our group. No significant effect was found. Therefore, the expected marginal improvement in accuracy would not justify the possible expensive undertaking of the simultaneous solution of electric field and the temperature profiles for the present truly three dimensional situation. In the present computations temperature independent thermal and electrical conductivities are used.

Isopotentials—Differences between ESW and ESR. Figure 2 illustrates the isopotentials along the half-midplanes between the welded plates and the copper shoes used in the ESW process for the experimental situation described in Table I. It will be noted that the isopotentials intersect the cooling shoe boundary at right angles but generally lie parallel to the metal plate boundary. This is due to the assumption of an insulating solidified slag layer on the surface of the water-cooled shoes, hence all of the welding current flows through the plates and the weld pool and none passes through the copper shoes. This situation is significantly different from the electroslag refining process (Fig. 3) where the current flows through the molten metal pool.

Table I. Values of Various Parameters Used for the Calculations

Thickness of the plates	0.038 m
Gap between the plates	0.019 m
Depth of slag	0.022 m
Distance between the top slag surface and the electrode tip	0.011 m
Radius of the electrode	0.0015 m
Radius of the electrode guide	0.005 m
Electrical conductivity of the slag (σ)	337.5 $(ohmm.m)^{-1}$

Table II. Values of Various Parameters Used for the Calculation of Temperature Fields

Plate thickness	2.5×10^{-2} m
Initial plate gap	3.0×10^{-2} m
Electrode radius	1.2×10^{-3} m
Metal drop radius	1.2×10^{-3} m
Depth of the slag pool	3.0×10^{-2} m
Electrode immersion in the slag	1.5×10^{-2} m
Metal pool geometry	See Fig. 8
Electrode voltage	37 V
Current	500 A
Molten slag electrical conductivity	375 $(Ohm.m)^{-1}$
Molten slag thermal conductivity	2.5×10^{-3} kcal/(ms K)
Molten metal thermal conductivity	5.0×10^{-3} kcal/(ms K)
Heat transfer coefficient at the slag/mold interface	0.04 kcal/(m^2s K)
Specific heat of the electrode	0.16 kcal/kg K
Specific heat of the liquid metal drops	0.2 kcal/kg K
Specific heat of the slag	0.25 kcal/kg K
Latent heat of fusion of the electrode	65 kcal/kg
Emissivity of the free slag surface[4]	0.6
Viscosity of the slag[4]	1.0×10^{-2} kg/(ms)
Density of liquid metal	7×10^3 kg/m^3
Density of liquid slag	2.7×10^3 kg/m^3
Effective conductivity of the slag phase	6.0×10^{-2} kal/(ms K)
Effective conductivity of the metal phase	3.0×10^{-2} kcal/(ms K)

In the ESW process, the contact of the molten slag with the base plates reduces the overall electrical resistance of the system and allows a much higher current. For a typical situation, this difference results in a 70 pct increase of the current used during ESW compared with the current which would be required in ESR with equivalent slag, electrode and other geometrical variables. This difference is fundamental to the ESW process and results in a much higher heat input than is necessary for melting of the electrode alone.

Heat Generation Patterns and Electrode Asymmetry. Knowledge of the isopotentials and the current distribution permits calculation of the heat generation patterns for the process, which is shown in Fig. 4. It will be noted that the intensity of heat generation near the electrode can be up to an order of magnitude greater than the heat generated near the slag-plate interface. The magnitude of variation is significantly larger in the direction of the cooling shoe. While this heat is transported throughout the slag by conduction and convection, the computation illustrates the great importance of electrode placement in determining the heat generation pattern when the electrode is displaced from the exact center of the slag pool. In Fig. 5 Q_x represents the integrated value of heat generation per unit plane width for x = constant planes.

$$Q_x = \int_{z_i}^{z_f} \int_{y_i}^{y_f} Q_g dy dz \qquad [12]$$

It is seen that by displaying the electrode by about 10 pct from the central planes of symmetry, significant asymmetry occurs in the heat generation pattern. While this imbalance in the heat generation intensity will be reduced somewhat by convective and diffusive transport of heat, the computation points out the need for the careful control of the electrode placement in the ESW process. It has been noted in our laboratory that excessive dilution of one plate may occur while producing lack of fusion of the second plate when the

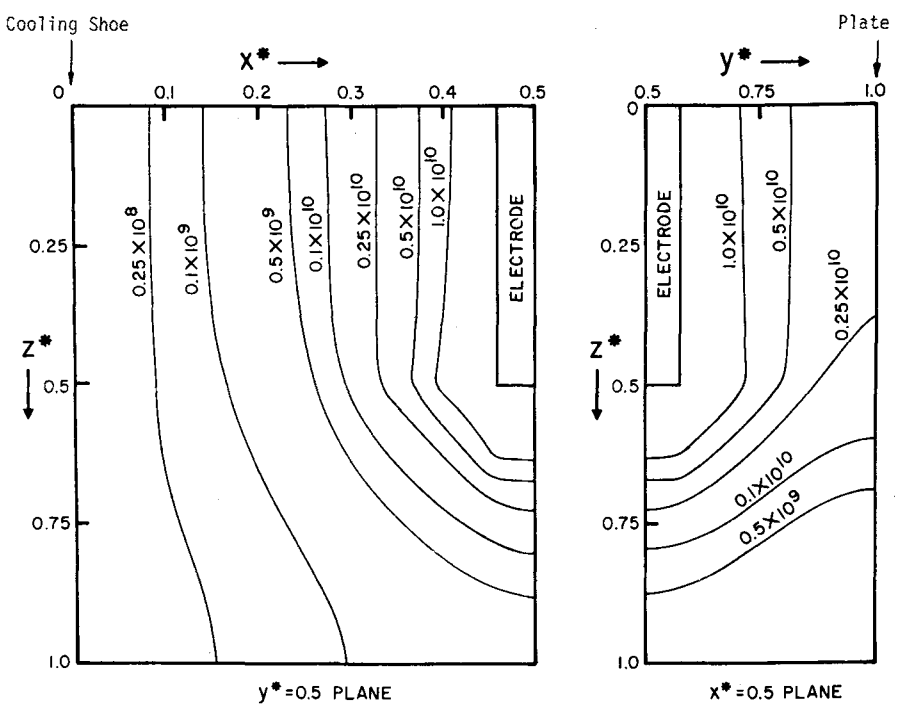

Fig. 4—Patterns of heat generation rate (in Watt/m^3) at two midsections.

electrode is not properly straightened. Even a small curvature of the electrode may cause welding defects, resulting from lack of fusion. The circular cross section of the cylindrical electrode was treated as a regular octagon in the computation scheme. The skewing in Fig. 5 is due to two factors. These factors are i) corner effects, and ii) at the center of the horizontal cross section of the electrode the voltage gradient is zero and consequently no heat is generated at this location. In the three electrode situation (Fig. 6) this effect is pronounced at $y^* = 0.5$ (the midplane which passes through the center of all the three electrodes) due to geometrical factors. In the $x^* =$ constant planes the effect is less pronounced due to the geometrical arrangement of the weld.

Multiple Electrodes. The three dimensional model permits an estimate of the effect of using multiple electrodes for ESW. The effect of very closely spaced electrodes on the local heat generation pattern is shown in Fig. 6.

The use of multiple electrodes produces a much more uniform heat generation especially when the electrodes

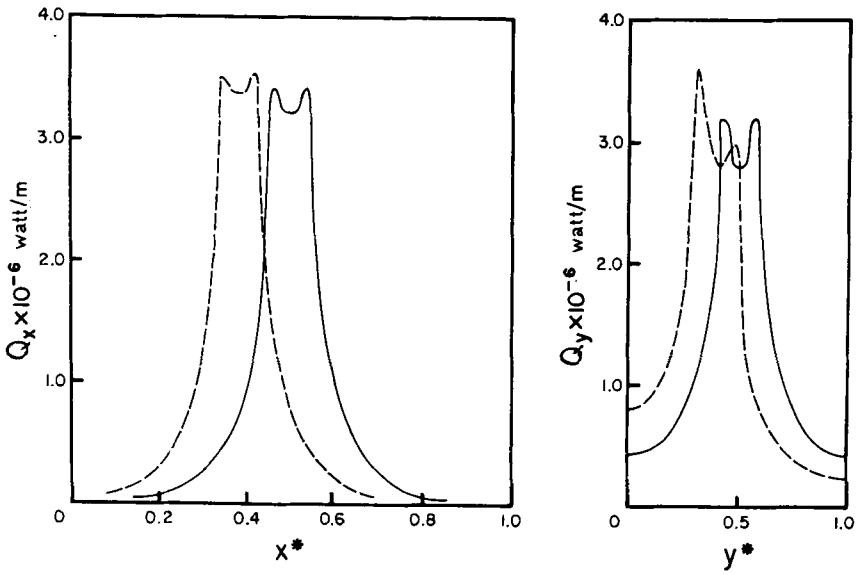

Fig. 5—Changes in heat generation pattern due to electrode asymmetry. The solid lines (—) represent the symmetrical case and the dotted lines (---) correspond to a case where the vertical axis of the electrode has been shifted to a location described by $(x_{elax} - x_i)/(x_f - x_i) = 0.38$ and $(y_{elax} - y_i)/(y_f - y_i) = 0.39$. (1 watt = 0.239 Kcal/s = 1 J/s).

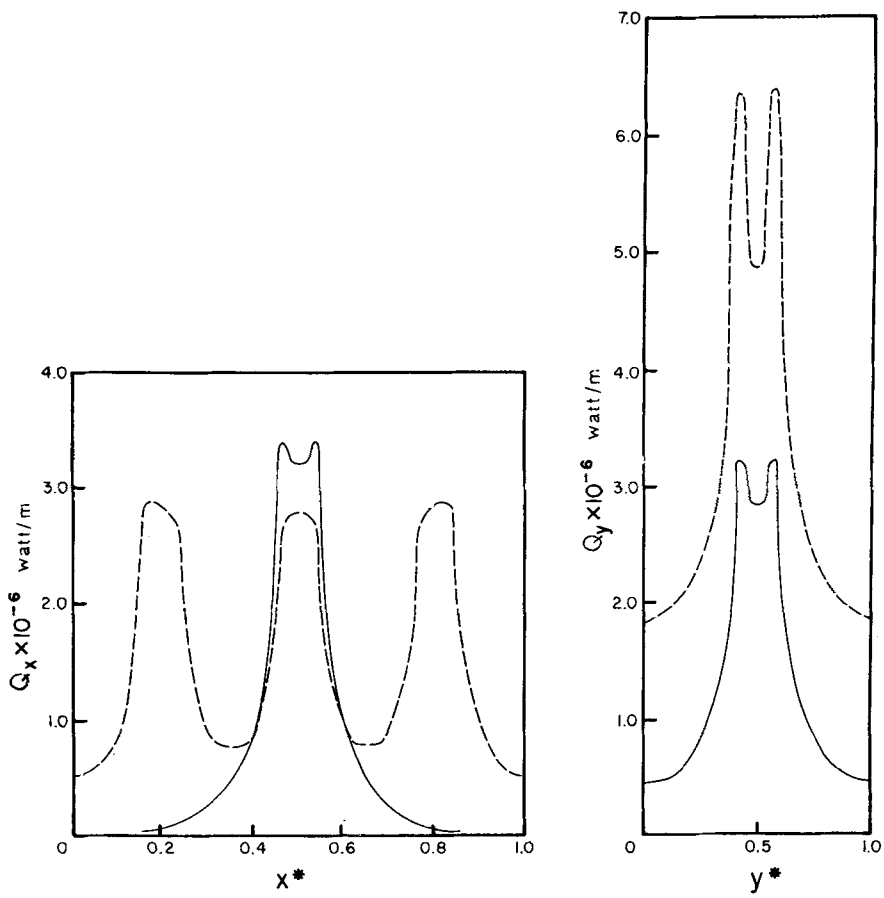

Fig. 6—Changes in heat generation pattern due to the use of multiple electrodes. The solid lines (—) represent the situation where a single electrode is used while the dotted lines (---) represent a situation where three electrodes are used. (1 watt = 0.239 Kcal/s = 1 J/s).

are closely spaced, *e.g.*, within two centimeters. To our knowledge, such close spacing of electrodes has not been attempted in ESW. Apparatus to test this prediction is currently being built and experimental results of this possible improvement in the ESW process should be available in the near future.

It may be appreciated at this stage why a single oscillating electrode[3] moving parallel to the plate surface can be used with success. First, on a time average basis, oscillation produces uniformity of heat input along the path of electrode movement. Secondly, agitation aids convective heat transfer thereby decreasing total temperature differences; accompanying turbulence also aids the heat transfer process.

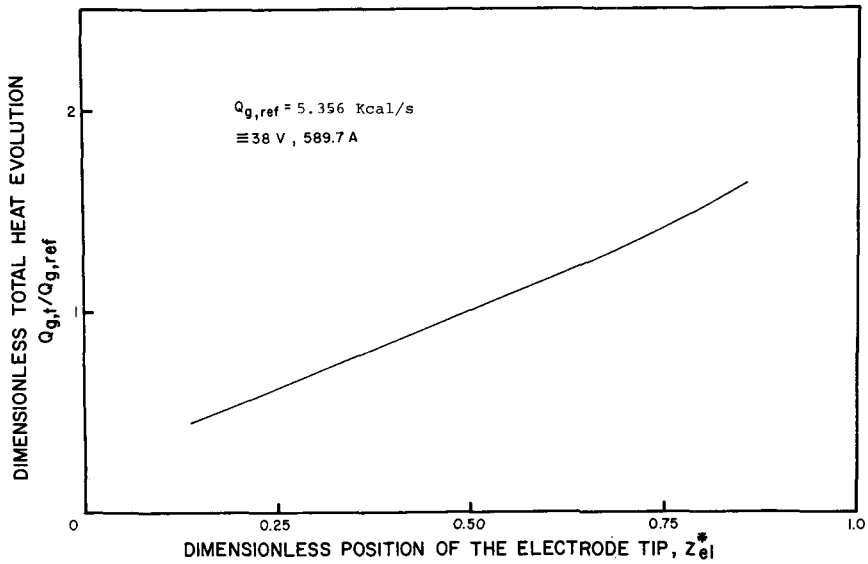

Fig. 7—Dimensionless position of the electrode tip, z^*_{el}. $[z^*_{el} = (z_{el} - z_i)/(z_{sm} - z_i)]$

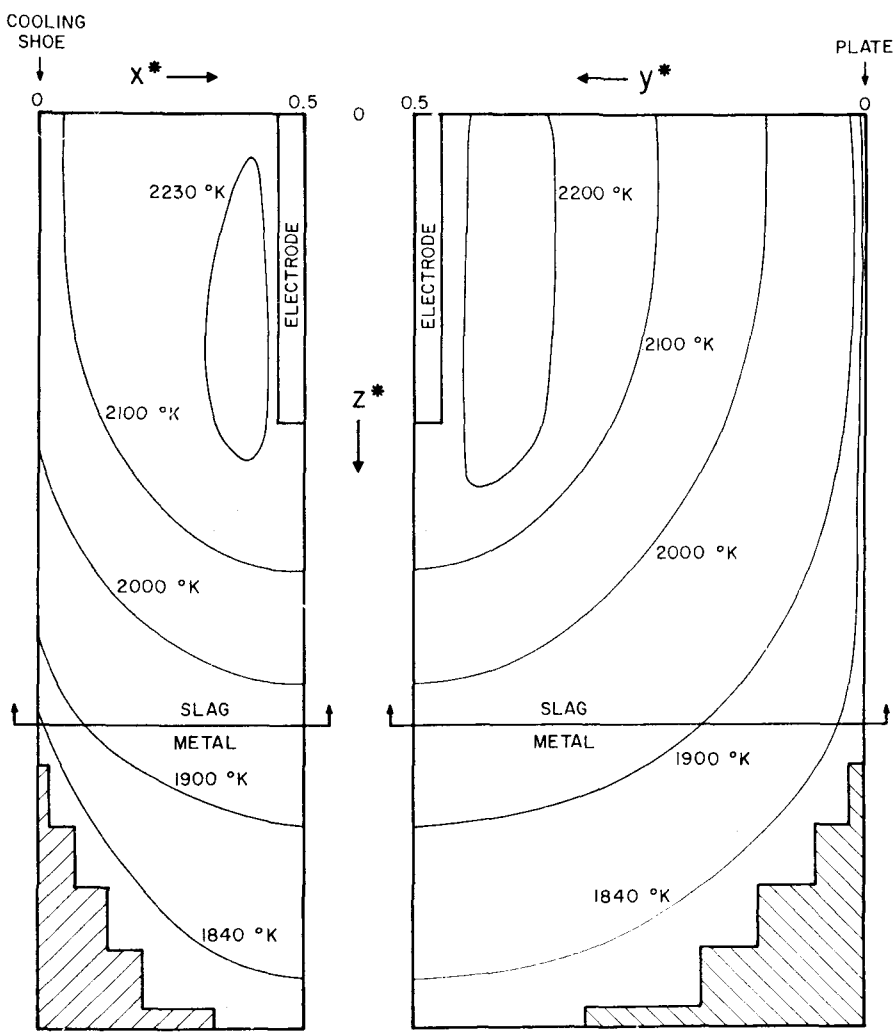

Fig. 8—Temperature profile at 'midsections'.

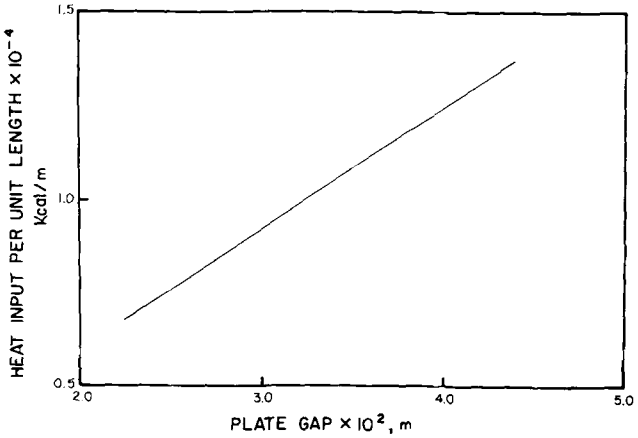

Fig. 9—Effect of plate gap on the heat input.

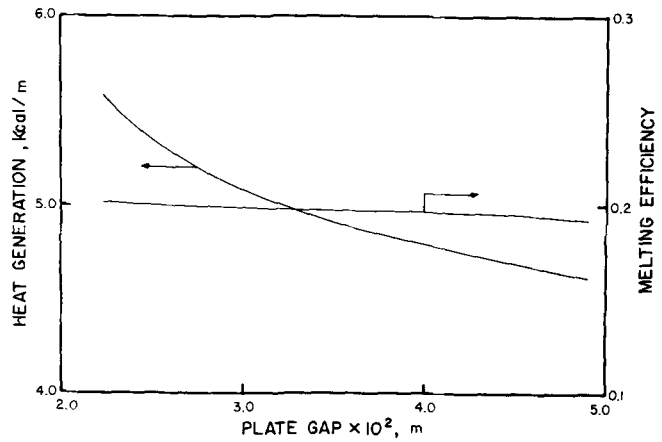

Fig. 10—Effect of plate gap on the total heat generated and melting efficiency. Melting efficiency is defined as the ratio of heat required for the heating and melting of the electrode to the total heat generated.

Penetration of the Electrode. In Fig. 7, the calculated value of total heat generation is plotted as a function of the depth of immersion of the electrode. It is observed that the welding current increases with an increase in the depth of immersion. This produces a self-stabilizing effect on the process as deviations in the vertical position of the electrode tip will change the rate of heat generation in such a way as to approach the original position.

Temperature Profiles. Although work is progressing on extension of the three-dimensional model to include the effects of convection explicitly, estimates of the temperature distribution may be made by solving the heat conduction equations using effective thermal conductivities. This approach of representing convection effects, albeit approximately by using effective conductivities or diffusivities, has been used extensively in the metallurgical literature.[5,6] Values of enhanced conductivity and other parameters used for the computation are listed in Table II. Values of the enhanced conductivities have been taken from the works of Dilawari, Szekely and Eagar[4] and are consistent with the vigorous slag convection found in ESW. The numerical values of the effective conductivity are also comparable to those used by Elliott and Maulvault.[5] The calculated values of isotherms in the slag and the metal phases are shown in Fig. 8. It is seen that the

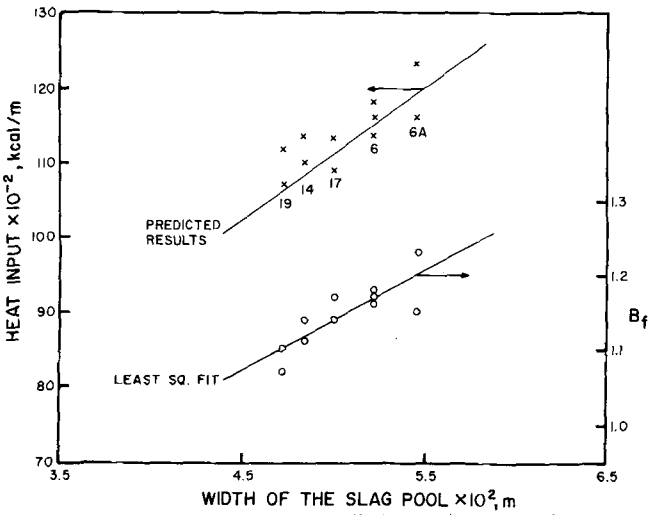

Fig. 11—Experimental and model predictions of heat input during welding.

temperature gradient near the cooling shoes is higher than near the base plates. Also the slag is hottest in the central region near the electrodes. The predictions of the model regarding the role played by various factors in the consumption and transport of energy in the slag phase is presented in Table III. It is seen that a large amount of heat is transported from the slag to the cooling shoes. For the geometrical situation considered, the amount of heat transported to the cooling shoes is larger than that reaching the plates, due to a relatively small plate thickness and a large gap between welding surfaces.

Some of the energy used in ESW will be consumed in the electrolysis of the flux, however the amount of energy consumed in this way is rather difficult to estimate. This is due to several factors including the lack of data on the activities of the various species, the possibility of numerous complex exchange reactions and the presence of a recirculating load of metals forming oxides near the anode and dissolving in the slag. Preliminary calculations reveal that the energy loss could range between 3 to 14 pct of the total power input for the conditions of experiments described in Table II. In the present calculations, a power loss of 10 pct has been allowed for the electrolysis of the molten flux.

Table III. Energy Balance in the Slag Phase

Item	Pct of Energy Dissipated
Heat transfer from slag to copper shoe	36.10
Heat transfer from slag to base plates	20.22
Heat transfer from slag to liquid metal	8.71
Heat used to heat the electrode to its melting point	15.26
Heat required to melt the electrode	4.07
Heat required to heat flux cooling on the consumable guide	1.84
To metal by liquid metal drops	2.04
Radiation loss from the slag surface	1.75
Electrochemical loss	10.00

Actual width of the slag pool 4.4×10^{-2} m, current 534 A, other conditions are the same as that presented in Table II.

Comparatively less heat is transported from the slag to the metal phase by the molten metal drops as the temperature at the slag/metal interface nearly equals the temperature of the slag at the slag/metal interface in the central region of the slag phase. An increase in the assumed diameter of the drop by 100 pct has an insignificant influence on the temperature field and the heat balance.

Consumable guides are normally coated with fluxes. In the present computations account has been made of the energy requirements for the heating of this cold flux or any other cold flux that is charged manually during the welding process. The energy requirement for heating of the fluxes is found to be about 2 pct of the total energy consumption.

Plate Gap. Some of the principal drawbacks normally ascribed to the ESW process include poor process control and excessive thermal energy input. The detrimental effect of the high heat input on the base metal properties, particularly fracture toughness, is probably the greatest hindrance to more widespread use of this potentially useful welding technique. An objective of this study has been to develop a means of achieving a reduction in the total thermal energy requirements of the process. One obvious way of achieving this is to reduce the plate gap. This follows because a reduction in the nominal gap requires less electrode to be melted per unit length, thus allowing a more rapid welding speed and a reduction in heat input.

Figure 9 shows the effect of the plate gap on the heat input for a situation in which there is negligible base metal dilution. It is seen that the rate of heat generation decreases with increasing plate gap, but the efficiency of electrode melting remains essentially constant. A decrease in plate gap is thought to be desirable because it promotes a favorable solidification pattern which must be maintained in the fusion zone. This requires a shallow weld pool, which produces a desirable form factor. Shallow weld pools at high welding speeds may only be achieved with reduced weld gaps, hence the conclusion that welding heat input is linearly related to plate gap suggests that the desirable ten-fold reduction in welding heat input can be obtained only by use of a very narrow gap. It is likely that gaps of such small size are impractical. Nonetheless, reductions of two or three times the typical welding heat input are possible in ESW with narrowed gaps and may be practical with very good process control. While such reductions would not be expected to be helpful for joining of pressure vessel steels, several new high heat input structural steels may benefit from a narrow gap electroslag welding process.[7,8]

Comparison with the Experimental Data. It is always desirable, in fact, essential to compare theoretical predictions with actual experimental measurements. In the present case, this comparison will be made with results reported by Benter *et al.*[3] For is not the same as the original plate spacing or nominal gap due to base heat input, two points are to be considered. The width of the slag pool is not the same as the original plate spacing or nominal gap due to base metal dilution. The real width of the slag pool is measured by examining the fused area. Also, the real welds bulge sideways and the amount of liquid metal necessary to carry out welding is higher than that required to fill the geometric shape of the cavity. This effect can be readily taken into account by calculation of a factor, B_f defined by the following relationship: B_f = (weight of metal deposited from the guide and the electrode wire)/(weight of metal necessary to fill the initial shape of the welding cavity).

$$B_f = \frac{u_w A_g + u_{el} A_{el}}{u_w A_{ca}} \qquad [13]$$

where A_g, A_{el} and A_{ca} are the area of cross-section of consumable guide, the wire electrode and the weld cavity (horizontal) respectively (in m^2), u_w is the weld rate in m/s, u_{el} is the linear velocity of the electrode in m/s.

For this same initial separation of plates, deeper slag pools provide a greater area of the heated plate and hence greater dilution. Electrode melting rates, however, are relatively insensitive to the slag depth. For the same nominal plate gap, the heat input is plotted with the width of the slag pool in Fig. 11. Experimental values of B_f are also included in this diagram. Data used for these calculations are presented in Table IV.

Table IV. Experimental Values of the Wire Feed Rate, Welding Rate, Bulging Factor and Heat Input (from Ref. 3)

Run Number	Slag Width m × 10^2	Weld Rate m/s × 10^4	Wire Feed Rate m/s × 10^2	Heat Input Kcal/m × 10^{-4}	Bulging Factor B_f
6A	5.5	3.58	5.97	1.233	1.23
		3.81	5.88	1.162	1.15
6	5.2	3.75	5.88	1.181	1.17
		3.38	5.93	1.308	1.28
		3.89	6.05	1.139	1.16
		3.81	6.05	1.162	1.18
17	5.0	3.89	6.14	1.135	1.17
		4.06	6.18	1.092	1.14
14	4.8	3.49	6.05	1.270	1.27
		3.88	5.93	1.139	1.14
		4.00	5.88	1.101	1.11
19	4.7	4.14	6.05	1.120	1.10
		4.32	6.05	1.073	1.07

Table V. The Effect of Variation of the Effective Conductivity Values on the Important Welding Variables

Serial Number		Effective Thermal Conductivity Kcal/m Ks Bulk	Near Wall	Heat Input $\times 10^{-2}$ Kcal/m	Finishing Time s	Maximum Local Slag Temperature K	Melting Rate $\times 10^3$ Kg/s	Pct of Total Energy Conducted to the Plates
1	Slag	0.075	0.075	91	589	3367	4.5	7.5
	Metal	0.150	0.150					
2	Slag	0.4	0.075	119	769	2474	3.4	18.2
	Metal	0.2	0.150					
3	Slag	0.6	0.075	137	769	2474	3.0	20.4
	Metal	0.3	0.150					
4	Slag	0.8	0.075	154	995	2250	2.7	21.5
	Metal	0.4	0.150					
5	Slag	0.6	0.075	137	881	2339	3.0	21.3
	Metal	0.2	0.150					
6	Slag	0.6	0.075	138	894	2331	3.0	19.8
	Metal	0.4	0.150					

Plate gap = 4.4×10^{-2} m, Nominal gap = 4.4×10^{-2} m $B_f = 1.0$, Current = 534 A, Weld length = 0.3 m. All the other conditions are listed in Table II.

The predicted values of heat input are seen to be in good agreement with the experimental results.

The depth of slag can be shown to have a direct effect on the amount of dilution of the weld metal. Deeper slag pools provide a greater contact area of heated base plate and hence greater dilution. Since the plate gap as described herein is based upon weld pool gap and not nominal base plate separation, reductions in weld heat input require the lowest possible slag pool depths capable of suppressing arcing. This will provide a weld of least possible dilution and smallest weld width (gap).

The Effect of an Externally-Imposed Magnetic Field on the Thermal Energy Input. The mathematical modelling work presented here enables one to obtain a preliminary estimate of the possible role that may be played by an externally imposed electromagnetic field on the total thermal energy input to the plate. In short, an externally-imposed field could be used, either to increase the agitation in the molten regions, or to suppress convection. These effects may be represented, albeit approximately by assigning different values to the effective thermal conductivities to the molten slag and metal regions. Table V lists the effects of variation of the bulk values of conductivity on important welding parameters like the heat input, weld finishing time (or weld rate) and so forth. It is observed that a decrease in the effective conductivity of the slag phase is accompanied by a reduction in heat input. In the following we shall discuss the implications of the reduction of effective conductivity of the slag.

For the same amount of heat generated in the slag, a decrease in the effective slag conductivity would decrease the local transport of the heat generated. This will result in an increase in the local temperatures and consequently cause an increase in the electrode melting rate since most of the heat is generated in the proximity of the electrode (Fig. 4). In the present work it has been found that an effective thermal conductivity in the slag equalling 24 times the molecular value fits the experimental data of heat input (Fig. 11). However, if the conductivity values in the slag and metal phases could be reduced to only three times the molecular values, a substantial reduction in the heat input would result (about 30 pct), although this would also produce unrealistically high temperatures in the slag phase. It is also seen from Table V that a decrease in the effective conductivity of the slag also decreases the proportion of the total energy transported to the vertical side of the base plates in contact with the slag for one inch thick plates.

Unlike in the slag phase, a change in the effective conductivity in the metal phase does not influence the key welding parameters as can be seen in Table V. This finding is consistent with the physical reasoning that in a typical situation only about 9 pct of the total energy is transported directly from the slag to the metal across the slag/metal interface (Table III).

CONCLUDING REMARKS

A mathematical formulation has been presented to calculate the three-dimensional heat generation patterns and temperature profiles in the electroslag welding process. The formulation involves the solution of the electric field equations, which in turn yields the local heat generation patterns. These heat generation patterns are in turn used to solve the three-dimensional heat conduction equation, using effective thermal conductivities to represent the convection process.

The principal findings of the modelling work are summarized in the following:

1) It is shown that in an ESW operation significantly higher currents are produced than in the electroslag refining process, principally because there is no solid slag cover on two of the side walls (which are melting base plates) resulting in a shorter current path.

2) The calculations show that the local heat generation patterns are extremely sensitive to the electrode location and even minor misalignment of the electrode may result in markedly asymmetrical heat generation patterns.

3) The use of multiple electrodes is found to indicate rather more uniform heat generation patterns.

4) The theoretical predictions based on the model are

found to be in reasonable agreement with experimental measurements reported in the literature.

5) Finally, through the use of the model it is possible to explore means for reducing the net heat input—a crucial objective in the improvement of the ESW process. The narrowing of the weld gaps, and the use of externally imposed electromagnetic fields to suppress convection, have both been investigated. With careful process control, reductions of two or three times the usual heat input may be practical.

APPENDIX A

I. Boundary conditions for the calculation of the voltage distribution values in the slag phase

Guide not in contact with the slag

Electrode:

$\phi = \phi_{el}$ for all values of x, y and z subject to

$z < z_{el}$

and

$$d \leq r_{el} \qquad [A1]$$

where

$$d = [\,(x - x_{elax})^2 + (y - y_{elax})^2\,]^{1/2}$$

Top slag surface:

$$\frac{\partial \phi}{\partial z} = 0 \text{ for } z = z_i$$

for all values of x and y. [A2]

Slag-metal surface:

$$\phi = 0 \text{ for } z = z_{sm}$$

for all values of x and y. [A3]

Side walls:

$$\frac{\partial \phi}{\partial x} = 0 \text{ for } x = x_i \text{ and } x = x_f$$

for all values of y and z [A4]

$$\phi = 0 \text{ for } y = y_i \text{ and } y = y_f$$

$$\left[\text{for ESR } \frac{\partial \phi}{\partial y} = 0\right]$$

for all values of x and z. [A5]

Guide touches the top slag surface

Top slag surface:

$$\phi = \phi_{el} \text{ for } z = z_i$$

and $d \leq r_g$ [A6]

$$\frac{\partial \phi}{\partial x} = 0 \text{ for } z = z_i$$

and $d > r_g$ [A7]

All other boundary conditions are the same as that mentioned earlier.

Multiple electrode guide not in contact with the slag

Electrode:

$\phi = \phi_{el}$ for all values of x, y and z

subject to $z \leq z_{el}$

and $d_i \leq r_{el}$ [A8]

where

$$d_i = [\,(x - x_{elxx,i})^2 + (y - y_{elax,i})^2\,]^{1/2}$$

for all values of i, where i is the index for the electrodes. All other boundary conditions are the same as that mentioned earlier.

II. Boundary conditions for the calculation of temperature profiles

Top slag surface:

$$k_{eff,sl} \frac{\partial T}{\partial z} = \frac{1}{2} \epsilon \sigma_s T^4 \qquad [A9]$$

Plate surface/slag interface:

$T = T_{lm}$ at $y = y_i$ and $y = y_f$

for all values of x and z. [A10]

Cooling shoe/slag interface:

$$k_{eff,sl} \frac{\partial T}{\partial x} = h_{ov} (T - T_a) \qquad [A11]$$

Slag/liquid metal interface

$$k_{eff,sl} \left.\frac{\partial T}{\partial z}\right|_{sl} = k_{eff,m} \left.\frac{\partial T}{\partial z}\right|_{m} \qquad [A12]$$

Liquid metal/plate interface

In the present computations, the liquid metal pool shape was prescribed to be approximately hemispherical. At the solid/liquid metal interface

$$T = T_{lm} \qquad [A13]$$

APPENDIX B

Calculation of Q_d, the amount of heat transported from slag to metal by the liquid metal drops

Metal drops formed as a result of the melting of the electrode absorb heat from the slag in the course of their downward journey. Rate of heat absorption by a single droplet and its temperature rise are given by the following relationships.

$$Q_{d,s} = 4\pi r_d^2 h_c (T - T_d) \qquad [B1]$$

$$\frac{4}{3} \pi r_d^3 \rho_d C_{pm} \frac{dT_d}{dt} = Q_{d,s} \qquad [B2]$$

Using the above relationships, the temperature change of the drop along its vertical path of descent is given by

$$\frac{u_d r_d \rho_d}{3} C_{pm} \frac{dT_d}{dz} = h_c (T - T_d) \qquad [B3]$$

$$T_d = T_{lm} \text{ at } z = z_{el} \qquad [B4]$$

$$T_d = T_f \text{ at } z = z_{sm} \qquad [B5]$$

and

$$\frac{2h_c r_d}{k_{eff,sl}} = 2 + 0.6\,\mathrm{Re}^{1/2}\mathrm{Pr}^{1/3} \qquad [B6]$$

Velocity of the liquid metal drops

As the drop descends along its path, its velocity changes. If one assumes that the velocity of the drop is significantly larger than that of the slag, so that the slag could be treated as stagnant compared to the drop, the velocity of the drop with time can be described by the equation

$$\frac{1}{u_d}\left(\rho_d + \frac{\rho_{sl}}{2}\right)\frac{du_d}{dz} = (\rho_d - \rho_{sl})g - \frac{3}{8}\frac{\rho_d}{r_d}C_D u_d^2$$

with

$$u_d = u_d^o \quad \text{at } z = z_{el} \qquad [B7]$$

The drag coefficient C_D appearing in the above equation is prescribed by using the available generalized results of independent earlier work. The specific relationships used are

$$C_D = 18.5/\mathrm{Re}^{3/5} \quad \text{for} 2 < \mathrm{Re} < 500$$
$$= 0.44 \quad \text{for Re} > 500 \qquad [B8]$$

Using these equations, Eq. [B3] can now be integrated to evaluate T_f at $z = z_{sm}$.

The rate of heat transport from the slag to the metal phase is therefore given by:

$$Q_d = mC_p(T_f - T_{lm}) \qquad [B9]$$

LIST OF SYMBOLS

A_g, A_{ca}, A_{el}	Area of cross section of the consumable guide, the weld cavity (horizontal) and the welding wire respectively, m^2
B_f	Defined by Eq. [13].
C_D	Drag coefficient
C_{pm}, C_{psl}	Specific heat of the metal and the slag respectively, kcal/kg K
d, d_i	Distance from the axis of the electrode and the corresponding value for the "i th" electrode respectively, m
E	Electric field, V/m
g	Acceleration due to gravity, m/s^2
h_c	Heat transfer coefficient at the metal droplet surface, kcal/m^2s K
h_{ov}	Overall heat transfer coefficient at the slag-copper shoe interface, kcal/m^2s K
ΔH_m, ΔH_{sl}	Latent heat of fusion of the metal and the slag respectively, kcal/kg
J	Current density Amp/m^2
k_{eff}	Effective thermal conductivity, kcal/ms K
m	Electrode melting rate, kg/s
Pr	Prandtl Number
Q_d	Heat transfer rate from the molten slag to metal by liquid metal drops, kcal/s
$Q_{d,S}$	Heat transfer rate to a single metal drop, kcal/s
Q_{elch}	Heat equivalent of the energy loss due to electrochemical effects, kcal/s
Q_{el}, Q_{slcu} Q_{slm}, Q_{slpl}	Heat transfer rate from the slag to the electrode, copper shoe, molten metal and the base plates respectively, kcal/s
Q_g, Q_s	Local values of the heat generation and heat loss rates respectively, kcal/m^3s
Q_{sl}	Total heat required to heat the cold slag, kcal
Q_{slr}	Heat required per unit time to heat the cold slag, kcal/s
Q_r	Rate of heat loss by radiation from the surface of the liquid slag, kcal/s
Q_t	Total power dissipation rate kcal/s
r_d, r_{el} and r_g	Radius of the liquid metal droplet, electrode wire and the guide respectively, m
Re	Reynolds number
T, T_a, T_d T_f, T_{lm}	T refers to temperature in the computation domain; subscripts a, d, f, and m refer to ambient temperature, metal drop temperature, value of metal drop temperature at the slag/metal interface and melting point of the metal, respectively, K
t, t_{fin}	Time and the time required to finish the weld, s
u_d	Velocity of the liquid metal drops, m/s
u_w	Weld rate, m/s
V_m	Volume of the liquid metal pool, m^3
W_{sl}	Total weight of slag charged during the weld, kg
W_{slr}	Rate of slag charge, kg/s
x, x_{elax} x_i and x_f	x-coordinate, the x-coordinate of the electrode axis and the beginning and the end x coordinates of the computation domain respectively, m
x^*	dimensionless distance in x direction, $(x - x_i)/(x_f - x_i)$
y, y_{elax} y_i, y_f	y-coordinate, the y-coordinate of the electrode axis, the beginning and the end y-coordinates of the computation domain respectively, m
y^*	dimensionless distance in y direction, $(y - y_i)/(y_f - y_i)$
z, z_{el}, z_i, z_f and z_{sm}	z-coordinate, the z-coordinate of the electrode tip, the beginning and the end coordinates of the computation domain and the z-coordinate of the slag/metal interface plane respectively, m
z^*	dimensionless distance in z direction, $(z - z_i)/(z_f - z_i)$
ρ_d, ρ_{sl}	Density of the liquid metal drop and the slag respectively, kg/m^3
σ, σ_s	Electrical conductivity of the slag, $(\text{ohm m})^{-1}$ and the Stephen-Boltzmann's constant respectively
ϵ	Emissivity of the free slag surface
ϕ, ϕ_{el}	Electrical potential at any point in the domain of computation and the electrical potential at the electrode respectively, V

ACKNOWLEDGMENTS

The authors wish to thank the U.S. Department of Energy for partial support of this investigation under Contract No. 87666.

REFERENCES

1. B. E. Paton: *Electroslag Welding*, American Welding Society, New York, 1962.
2. J. D. Harrison: *Met. Constr. Br. Weld. J.*, vol. 1, no. 8, August 1969, pp. 366–70.
3. W. P. Benter, Jr., P. J. Konkol, B. M. Kapadia, A. K. Shoemaker, and J. F. Sovak: *Acceptance Criteria for Electroslag Weldments in Bridges, Phase I.* Final Report, U.S. Steel Corporation, Monroeville, PA, April 1977, p. A-5.
4. A. H. Dilawari, J. Szekely, and T. W. Eagar: *Weld. J.*, January 1978, vol. 58, no. 1, p. 24s.
5. J. F. Elliott and M. A. Maulvault: *Elec. Furnace Conf. Proc.*, vol. 28, p. 13, AIME, New York, 1970.
6. A. S. Ballantyne and A. Mitchell: *Ironmaking Steelmaking*, 1977, no. 4, p. 222.
7. U.S. Patent 4,025,368, Kawasaki Steel Corporation, May 30, 1975.
8. U.S. Patent No. 3,773,500, Nippon Steel Corporation, March 24, 1971.
9. J. Szekely and M. Choudhary: Unpublished research, Department of Materials Science and Engineering, MIT, Cambridge.